Effects of counter-rotating couplings of the Rabi model with frequency modulation

Yiying Yan,[1,*] Zhiguo Lü,[2,3,†] JunYan Luo,[1] and Hang Zheng[2,3,‡]

[1]*Department of Physics, School of Science, Zhejiang University of Science and Technology, Hangzhou 310023, China*

[2]*Key Laboratory of Artificial Structures and Quantum Control (Ministry of Education), Department of Physics and Astronomy, Shanghai Jiao Tong University, Shanghai 200240, China*

[3]*Collaborative Innovation Center of Advanced Microstructures, Nanjing 210093, China*

(Received 7 May 2017; published 1 September 2017)

We theoretically study the dynamics and resonance shift of the Rabi model with frequency modulation, i.e., the Rabi model driven additionally by a slow longitudinal field, by using the counterrotating-hybridized rotating-wave (CHRW) method, aiming to illustrate the effects of the counterrotating (CR) terms of the transverse field. The CHRW method is based on a unitary transformation and reduces the aperiodic Hamiltonian to an effective periodic Hamiltonian that can be efficiently treated by Floquet theory. The validity of the effective Hamiltonian and widely used rotating-wave approximation (RWA) Hamiltonian is carefully examined compared to the numerically exact results over a wide parameter range. It is found that the effective Hamiltonian gives a correct description, while the RWA breaks down in the strong driving regime. Interestingly, we show that under certain conditions the longitudinal field can be used to modify resonance widths such that resonance widths can be comparable to the magnitude of the Bloch-Siegert (BS) shift, which in turn makes the CR-induced BS shift significant and leads to the complete breakdown of the RWA even in a moderately strong driving regime (in which the RWA holds for the Rabi model without frequency modulation). In addition, by using the effective Hamiltonian, we can efficiently access resonance positions for the bichromatically driven qubit and study how the resonance shifts due to the combined effects of the CR terms and frequency modulation. For a weak longitudinal field, we show that resonance positions can be analytically calculated from the effective Rabi frequency for the effective Hamiltonian, which are in excellent agreement with the numerically exact results.

DOI: 10.1103/PhysRevA.96.033802

I. INTRODUCTION

Recently, there is increased interest in studying driven quantum systems in the strong driving regime where the rotating-wave approximation (RWA) breaks down [1–9]. It follows from the development of artificial atoms that light-matter interaction in the strong- and ultrastrong-coupling regimes will become available in laboratories. For instance, strongly driven two-level systems with a Rabi frequency comparable to the transition frequency of the two levels have been experimentally realized in the context of the flux qubit [8,10]. Strong driving turns out not only to cause unique physical phenomena such as coherent destruction of tunneling [11] and Bloch-Siegert (BS) shift [12–14] but also to be useful in the fast quantum control of semiconductor qubits, which is essential for solid-state quantum computation [15,16].

The prototype of the driven quantum system is the Rabi model, which is described by ($\hbar = 1$)

$$\begin{aligned} H(t) &= \frac{1}{2}\omega_0\sigma_z + \Omega_x \cos(\omega_x t)\sigma_x \\ &= \frac{1}{2}\omega_0\sigma_z + \frac{\Omega_x}{2}(e^{i\omega_x t}\sigma_- + e^{-i\omega_x t}\sigma_+) \\ &\quad + \frac{\Omega_x}{2}(e^{-i\omega_x t}\sigma_- + e^{i\omega_x t}\sigma_+), \end{aligned} \tag{1}$$

where $\sigma_\pm = (\sigma_x \pm i\sigma_y)/2$ and $\sigma_{x,y,z}$ are the Pauli matrices. ω_0 is the transition frequency of the qubit. $\Omega_x \cos(\omega_x t)$ is the transverse driving field with amplitude Ω_x and frequency ω_x. This model is widely used in quantum optics [17] and has been extensively studied by numerically exact and analytical methods [13,18,19]. In the strong driving regime ($\Omega_x/\omega_0 \gtrsim 1$), one becomes concerned with the effects of the counterrotating (CR) terms [last line in Eq. (1)], which are neglected in the RWA. It is clear that the CR terms are to induce a complex beat in the real-time dynamics and the BS shift. The latter has been studied both theoretically [12,13,20] and experimentally in the context of superconducting qubits [21,22]. Due to the inevitable power broadening, one finds that the magnitude of the BS shift of the main resonance at $\omega_0 \approx \omega_x$ is generally much less than that of the resonance width, thus the BS shift can be neglected even when the driving is moderately strong.

It is interesting to investigate whether the resonance width can be significantly modified with additional driving such that the resonance width is comparable to the magnitude of the BS shift and how the BS shift influences the dynamics in this situation. To address these issues, we consider that the transition frequency in the Rabi model is modulated by a longitudinal field. The total Hamiltonian is given by

$$H(t) = \tfrac{1}{2}[\omega_0 + \Omega_z \cos(\omega_z t)]\sigma_z + \Omega_x \cos(\omega_x t)\sigma_x, \tag{2}$$

where $\Omega_z \cos(\omega_z t)$ is the longitudinal driving field with amplitude Ω_z and frequency ω_z. The model can be used to describe the magnetic resonance [23] and solid quantum optics experiments in the context of artificial atoms such as superconducting qubits [24] and nitrogen vacancy spin qubits [25]. As the limit case of the quantum Rabi model that a qubit interacts with two harmonic oscillators [25], it can be expected to provide a description physically equivalent to that with the

*yiyingyan@zust.edu.cn
†zglv@sjtu.edu.cn
‡hzheng@sjtu.edu.cn

fully quantized theory in the large-photon-number limit when the quantized fields are in coherent states, similar to the usual Rabi model [13]. In previous work, this model was studied with the aid of the RWA for the transverse field [23,24,26–28]. For instance, in Ref. [26], Saiko and coworkers have theoretically and experimentally studied the resonance shift resulting from the fast-oscillating terms of the longitudinal field, which is referred to as $\delta_{\rm d}$ shift henceforth, to distinguish it from another shift caused by the CR terms of the transverse field (in their paper, the $\delta_{\rm d}$ shift is called the BS shift). Clearly, the combined effect of the CR terms and the longitudinal field has not been illustrated because of the RWA.

It can be expected that the CR-induced BS shift in the bichromatically driven qubit described by Eq. (2) is much more significant than that in the standard Rabi model for the following reasons. First, it has been revealed that a qubit driven by a bichromatic field with two perpendicular components has multiple resonance peaks appearing at $\omega_0 \approx \omega_x + m\omega_z$ ($m = 0,\pm1,\pm2,\dots$) [24]. This is in sharp contrast with the usual Rabi model, where one finds only a single resonance peak at resonance position $\omega_0 \approx \omega_x$ [13]. It is therefore interesting to study the CR-induced BS shifts of the additional resonance peaks ($m \neq 0$). Second, it is found that the resonance peak at $\omega_0 \approx \omega_x$ can be narrower with longitudinal modulation than without longitudinal modulation [24]. Consequently, one may ask whether the widths of resonance peaks may reduce to the magnitude of the BS shifts in the presence of longitudinal modulation, which cannot be expected in the Rabi model at the main resonance, due to power broadening [29].

In this work, we use both the counterrotating-hybridized rotating-wave (CHRW) method and the numerically exact method to study the dynamics and resonance shifts of the Rabi model with the frequency modulation in the strong driving regime. The exact method is based on the generalized Floquet theory (GFT) [30]. The CHRW method is developed with a unitary transformation. It is applied to derive an effective Hamiltonian periodic in time so that methods for the periodically driven quantum system can be applied. The validity of the RWA Hamiltonian and our effective Hamiltonian is carefully examined by comparison with the exact transient and time-average transition probabilities obtained with the GFT. It is found that our effective Hamiltonian can provide a much more reliable description than the previous RWA one over a wide range of parameters. For moderately strong transverse driving, although the CR terms can be neglected in the absence of longitudinal field, it becomes essentially important when an elaborated longitudinal field is additionally applied. The longitudinal field can significantly reduce the resonance width to the magnitude of the BS shifts at the central band and sidebands, which in turn results in a dramatic difference in dynamics between the RWA and the non-RWA theories at the resonance positions given by the RWA. We find that well-approximated resonance positions that takes BS shifts into account can be efficiently calculated from our effective Hamiltonian. Without the RWA, the additional resonance peaks have both the BS shift and the $\delta_{\rm d}$ shift. In particular, when the longitudinal field is relatively weak, it is found that the resonance shift can be analytically calculated from the effective Rabi frequency for the effective Hamiltonian, and the result agrees well with the numerically exact result.

The remainder of the paper is organized as follows. In Sec. II, first we briefly review previous RWA treatment. Then we derive an effective periodic Hamiltonian by using the unitary transformation. The effective system is treated by the Floquet approach. In Sec. III, we introduce the GFT approach. In Sec. IV, we calculate the transient transition probability and examine the performance of the RWA and effective Hamiltonians by comparing their predictions with the exact ones and demonstrate that the longitudinal field can amplify the effects of CR terms on the dynamics. In Sec. V, by calculating the time-average transition probability, we clarify how the effects of the CR terms become significant under moderately strong transverse driving due to the longitudinal field and illustrate BS shifts at both the central band and the sideband in the moderately strong transverse driving regime. In Sec. VI, we give concluding remarks on this work.

II. EFFECTIVE HAMILTONIAN AND FLOQUET FORMALISM

A. Rotating-wave approximation

We first briefly review the RWA method used in previous work [23,24,26–28] to solve the time evolution governed by Eq. (2). Within the RWA, the Hamiltonian becomes

$$H_{\rm RWA}(t) = \frac{1}{2}[\omega_0 + \Omega_z \cos(\omega_z t)]\sigma_z + \frac{\Omega_x}{2}(\sigma_+ e^{-i\omega_x t} + \sigma_- e^{i\omega_x t}), \tag{3}$$

where the CR terms of the transverse field have been omitted. It is straightforward to further simplify the RWA Hamiltonian in the frame rotating at frequency ω_x, i.e.,

$$\begin{aligned}\tilde{H}_{\rm RWA}(t) &= R(t)H_{\rm RWA}(t)R^\dagger(t) - iR(t)\frac{d}{dt}R^\dagger(t)\\ &= \frac{\Omega_x}{2}\sigma_x + \frac{1}{2}[\delta + \Omega_z\cos(\omega_z t)]\sigma_z,\end{aligned} \tag{4}$$

where $R(t) = \exp(i\omega_x t\sigma_z/2)$ and $\delta = \omega_0 - \omega_x$ is the detuning of the transverse field from the static transition frequency. Clearly, Eq. (4) is corresponding to a periodically driven qubit, which can be solved by the Floquet approach [13]. Although the RWA simplifies the problem, it is expected to hold for near- and on-resonance cases and weak driving conditions ($\Omega_x \ll \omega_0$). Therefore, the validity of Eq. (4) becomes questionable in the strong driving regime, i.e., the driving strength of the transverse field becomes comparable to the transition frequency ω_0, in which case the CR terms are found to cause complex dynamics and a remarkable BS shift. To take into account the effects of the CR terms of the transverse field, we propose the use of a unitary transformation other than the RWA to derive an effective periodic Hamiltonian with a more precise description compared to the RWA one.

B. Unitary transformation

The evolution operator of a driven qubit satisfies the equation of motion

$$\frac{d}{dt}U(t) = -iH(t)U(t). \tag{5}$$

To go beyond the RWA, we perform the unitary transformation to the evolution operator [19,20,31]

$$U'(t) = e^{S(t)}U(t), \tag{6}$$

where

$$S(t) = i\frac{\Omega_x}{\omega_x}\xi \sin(\omega_x t)\sigma_x, \tag{7}$$

with ξ being undetermined. It is straightforward to show that the transformed evolution operator satisfies a similar equation $\frac{d}{dt}U'(t) = -iH'(t)U'(t)$ with the transformed Hamiltonian

$$\begin{aligned} H'(t) &= e^{S(t)}[H(t) - i\partial_t]e^{-S(t)} \\ &= \tfrac{1}{2}[\omega_0 + \Omega_z\cos(\omega_z t)]\{\cos[Z\sin(\omega_x t)]\sigma_z \\ &\quad + \sin[Z\sin(\omega_x t)]\sigma_y\} \\ &\quad + \Omega_x(1-\xi)\cos(\omega_x t)\sigma_x, \end{aligned} \tag{8}$$

where $Z = \frac{2\Omega_x}{\omega_x}\xi$. To proceed, we use the identity

$$\exp(iz\sin\theta) = \sum_{n=-\infty}^{\infty} J_n(z)e^{in\theta}, \tag{9}$$

where $J_n(z)$ is the Bessel function of the first kind with order n, and divide $H'(t)$ into two parts:

$$H'(t) = H'_{\mathrm{CHRW}}(t) + H'_2(t), \tag{10}$$

$$\begin{aligned} H'_{\mathrm{CHRW}}(t) &= \tfrac{1}{2}[\omega_0 + \Omega_z\cos(\omega_z t)]J_0(Z)\sigma_z + \omega_0 J_1(Z) \\ &\quad \times \sin(\omega_x t)\sigma_y + \Omega_x(1-\xi)\cos(\omega_x t)\sigma_x \\ &\quad + \tfrac{1}{2}J_1(Z)\Omega_z\cos(\omega_z t)(\sigma_+ e^{-i\omega_x t} + \mathrm{H.c.}), \end{aligned} \tag{11}$$

$$\begin{aligned} H'_2(t) &= [\omega_0 + \Omega_z\cos(\omega_z t)]\sum_{n=1}^{\infty}\{J_{2n}(Z)\cos(2n\omega_x t)\sigma_z \\ &\quad + J_{2n+1}(Z)\sin[(2n+1)\omega_x t]\sigma_y\} - \frac{1}{2}J_1(Z) \\ &\quad \times \Omega_z\cos(\omega_z t)(\sigma_+ e^{i\omega_x t} + \mathrm{H.c.}). \end{aligned} \tag{12}$$

Now we are in a position to determine the parameter ξ by requiring $H'_{\mathrm{CHRW}}(t)$ to take a rotating-wave form similar to $\tilde{H}_{\mathrm{RWA}}(t)$. To this end, we restrict ξ to the interval $(0,1)$ and determine its value via the following equation:

$$\Omega_x(1-\xi) = \omega_0 J_1(Z). \tag{13}$$

This equation can be solved numerically or analytically by Taylor expansion. When $\Omega_x/\omega_x < 1$, it is easy to find the expression for ξ accurate up to sixth order in Ω_x as follows:

$$\begin{aligned} \xi = \frac{\omega_x}{\omega_0+\omega_x}\Bigg[1 &+ \frac{\Omega_x^2\omega_0}{2(\omega_x+\omega_0)^3} + \frac{\omega_0(8\omega_0-\omega_x)\Omega_x^4}{12(\omega_x+\omega_0)^6} \\ &+ \frac{\Omega_x^6\omega_0\left(\omega_x^2 - 46\omega_x\omega_0 + 169\omega_0^2\right)}{144(\omega_x+\omega_0)^9}\Bigg] + O\left(\Omega_x^8\right). \end{aligned} \tag{14}$$

Using Eq. (13) and

$$\tilde{\Omega}_x = 2\Omega_x(1-\xi), \tag{15}$$

we can rewrite $H'_{\mathrm{CHRW}}(t)$ as

$$\begin{aligned} H'_{\mathrm{CHRW}}(t) &= \tfrac{1}{2}[\omega_0 + \Omega_z\cos(\omega_z t)]J_0(Z)\sigma_z + \tfrac{1}{2}[\tilde{\Omega}_x \\ &\quad + J_1(Z)\Omega_z\cos(\omega_z t)](\sigma_+ e^{-i\omega_x t} + \mathrm{H.c.}), \end{aligned} \tag{16}$$

which now takes the rotating-wave form. When $\Omega_z \to 0$, $H'_{\mathrm{CHRW}}(t)$ recovers the CHRW Hamiltonian for the monochromatically driven qubit [20,31].

To derive an effective periodic Hamiltonian, we use a treatment similar to the RWA method, namely, we transform the resulting Hamiltonian into a rotating frame with $R(t)$, yielding

$$\tilde{H}(t) = \tilde{H}_{\mathrm{CHRW}}(t) + \tilde{H}_2(t), \tag{17}$$

$$\begin{aligned} \tilde{H}_{\mathrm{CHRW}}(t) &= \tfrac{1}{2}\{[\omega_0 + \Omega_z\cos(\omega_z t)]J_0(Z) - \omega_x\}\sigma_z \\ &\quad + \tfrac{1}{2}[\tilde{\Omega}_x + J_1(Z)\Omega_z\cos(\omega_z t)]\sigma_x, \end{aligned} \tag{18}$$

$$\begin{aligned} \tilde{H}_2(t) &= [\omega_0 + \Omega_z\cos(\omega_z t)]\sum_{n=1}^{\infty}\{J_{2n}(Z)\cos(2n\omega_x t)\sigma_z \\ &\quad - iJ_{2n+1}(Z)\sin[(2n+1)\omega_x t](\sigma_+ e^{i\omega_x t} - \mathrm{H.c.})\} \\ &\quad - \frac{1}{2}J_1(Z)\Omega_z\cos(\omega_z t)(\sigma_+ e^{i2\omega_x t} + \mathrm{H.c.}). \end{aligned} \tag{19}$$

Up till now, the treatment is still exact without introducing any approximation. If ω_z is much smaller than ω_x, $\tilde{H}_{\mathrm{CHRW}}(t)$ includes the slow-varying terms with periodicity $T = 2\pi/\omega_z$, whereas $\tilde{H}_2(t)$ possesses the fast-oscillating terms. To proceed, we use $\tilde{H}_{\mathrm{CHRW}}(t)$ as the effective Hamiltonian.

We neglect $\tilde{H}_2(t)$ for the following reason. Physically, $\tilde{H}_2(t)$ is related to multiphoton processes assisted by photons of the transverse and longitudinal fields, i.e., it yields the multiphoton resonances that occur at $\omega_0 \approx n\omega_x + m\omega_z$ for $n = 3,5,7,\ldots$ and m any integer. When neglecting $\tilde{H}_2(t)$, we just retain the resonances that occur at $\omega_0 \approx \omega_x + m\omega_z$, similarly to the RWA treatment [24]. We can expect our treatment to be valid in the regime where the contribution from $\tilde{H}_2(t)$ is insignificant and negligible. Therefore, we should require that $J_n(Z) \ll 1$ ($n \geqslant 2$) and $J_1(Z)\Omega_z/\omega_0 \ll 1$ are fulfilled. Recalling the properties of the higher-order Bessel functions ($n \geqslant 2$) and the fact that $\xi < 1$, it is straightforward to verify that the first condition is met when $\Omega_x/\omega_x < 1$. Hence, if $\Omega_x/\omega_x < 1$, the validity of the effective Hamiltonian depends only on the second condition. In Fig. 1, we calculate the dimensionless amplitude $J_1(Z)\Omega_z/\omega_0$ as a function of the ratios Ω_z/ω_0 and Ω_x/ω_x. The blue area, $J_1(Z)\Omega_z/\omega_0 \lesssim 0.1$, represents the regime of the validity. It seems almost unchanged for the two values of the ratio ω_0/ω_x and does not depend on the value of ω_z as long as ω_z is smaller than ω_x. In Secs. IV and V, we demonstrate that in the valid regime, the effective Hamiltonian indeed provides a much better description than the RWA Hamiltonian.

C. Floquet formalism

Since the CHRW Hamiltonian is periodic in time, i.e., $\tilde{H}_{\mathrm{CHRW}}(t) = \tilde{H}_{\mathrm{CHRW}}(t+T)$, the corresponding time evolution operator $\tilde{U}_{\mathrm{CHRW}}(t)$ can be simply obtained by the Floquet

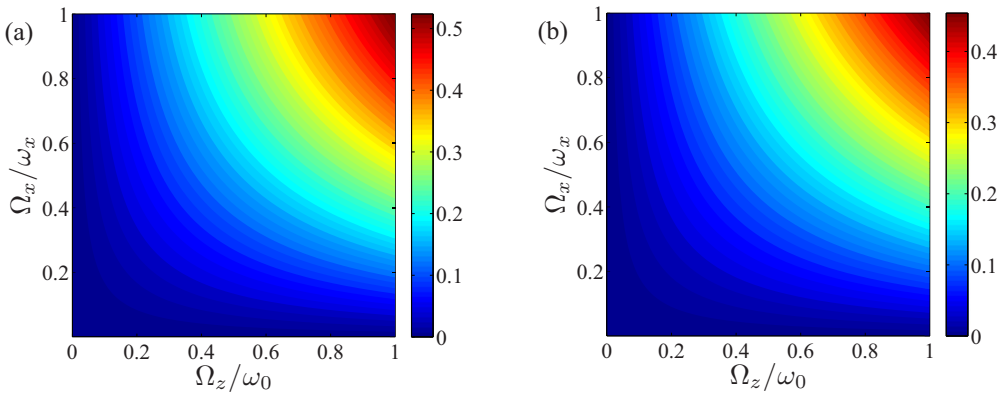

FIG. 1. Dimensionless amplitude $J_1(Z)\Omega_z/\omega_0$ versus the ratios Ω_z/ω_0 and Ω_x/ω_x for (a) $\omega_0 = 0.6\omega_x$ and (b) $\omega_0 = \omega_x$. The blue area represents the valid regimes of the effective Hamiltonian.

formalism and is assumed to take the form [13,32]

$$\tilde{U}_{\mathrm{CHRW}}(t) = \sum_{\gamma} |\tilde{u}_{\gamma}(t)\rangle\langle\tilde{u}_{\gamma}(0)|e^{-i\tilde{\varepsilon}_{\gamma}t}, \tag{20}$$

where $|\tilde{u}_{\gamma}(t)\rangle$ has the same periodicity as $\tilde{H}_{\mathrm{CHRW}}(t)$ and is called the Floquet state. $\tilde{\varepsilon}_{\gamma}$ is the corresponding quasienergy. By differentiating Eq. (20) with respect to t, one readily derives the equation that the Floquet state and quasienergy satisfy,

$$[\tilde{H}_{\mathrm{CHRW}}(t) - i\partial_t]|\tilde{u}_{\gamma}(t)\rangle = \tilde{\varepsilon}_{\gamma}|\tilde{u}_{\gamma}(t)\rangle. \tag{21}$$

This differential equation can be solved by Fourier expansion. We expand the CHRW Hamiltonian and Floquet state as follows:

$$\tilde{H}_{\mathrm{CHRW}}(t) = \sum_{n} \tilde{H}^{(n)}_{\mathrm{CHRW}} e^{in\omega_z t}, \tag{22}$$

$$\tilde{H}^{(n)}_{\mathrm{CHRW}} = \begin{cases} \frac{1}{2}\{[J_0(Z)\omega_0 - \omega_x]\sigma_z + \tilde{\Omega}_x\sigma_x\}, & n = 0, \\ \frac{1}{4}[J_0(Z)\sigma_z + J_1(Z)\sigma_x]\Omega_z, & n = \pm 1, \\ 0, & n \neq 0, \pm 1, \end{cases} \tag{23}$$

and

$$|\tilde{u}_{\gamma}(t)\rangle = \sum_{n} \left|\tilde{u}^{(n)}_{\gamma}\right\rangle e^{in\omega_z t}, \tag{24}$$

where

$$\left|\tilde{u}^{(n)}_{\gamma}\right\rangle = \frac{1}{T}\int_0^T e^{-in\omega_z t}|\tilde{u}_{\gamma}(t)\rangle dt \tag{25}$$

is a time-independent Fourier component of the Floquet state. By substituting Eqs. (22) and (24) into Eq. (21), one derives the algebra equation concerning the Fourier components and quasienergy, which reads

$$\sum_{n}\left[\tilde{H}^{(m-n)}_{\mathrm{CHRW}} + n\omega_z\delta_{n,m}\right]\left|\tilde{u}^{(n)}_{\gamma}\right\rangle = \tilde{\varepsilon}_{\gamma}\left|\tilde{u}^{(m)}_{\gamma}\right\rangle, \tag{26}$$

where $\delta_{n,m}$ is the Kronecker delta function. This equation can be further rewritten as

$$\tilde{\mathcal{H}}_{\mathrm{CHRW}}|\tilde{u}_{\gamma}\rangle\rangle = \tilde{\varepsilon}_{\gamma}|\tilde{u}_{\gamma}\rangle\rangle. \tag{27}$$

We have defined the Floquet matrix and its eigenstate as

$$\tilde{\mathcal{H}}_{\mathrm{CHRW}} = \begin{pmatrix} \ddots & \ddots & \ddots & & \\ \ddots & \tilde{H}^{(0)}_{\mathrm{CHRW}} - \omega_z\mathbf{1} & \tilde{H}^{(-1)}_{\mathrm{CHRW}} & \mathbf{0} & \\ \ddots & \tilde{H}^{(1)}_{\mathrm{CHRW}} & \tilde{H}^{(0)}_{\mathrm{CHRW}} & \tilde{H}^{(-1)}_{\mathrm{CHRW}} & \ddots \\ & \mathbf{0} & \tilde{H}^{(1)}_{\mathrm{CHRW}} & \tilde{H}^{(0)}_{\mathrm{CHRW}} + \omega_z\mathbf{1} & \ddots \\ & & \ddots & \ddots & \ddots \end{pmatrix}, \quad |\tilde{u}_{\gamma}\rangle\rangle = \begin{pmatrix} \vdots \\ |\tilde{u}^{(-1)}_{\gamma}\rangle \\ |\tilde{u}^{(0)}_{\gamma}\rangle \\ |\tilde{u}^{(1)}_{\gamma}\rangle \\ \vdots \end{pmatrix}, \tag{28}$$

respectively. Here $\mathbf{0}$ ($\mathbf{1}$) denotes a 2×2 zero (identity) matrix. Up till now, the problem of finding the Floquet states and quasienergies in Eq. (21) is converted into an eigenvalue problem, Eq. (27). One can diagonalize $\tilde{\mathcal{H}}_{\mathrm{CHRW}}$ numerically or analytically and use the knowledge of its eigenvalues (quasienergies) and eigenstates (consisting of Fourier components of Floquet states) to derive $\tilde{U}_{\mathrm{CHRW}}(t)$. Finally, the original evolution operator can be obtained with the relation

$$U(t) = e^{-S(t)}R^{\dagger}(t)\tilde{U}_{\mathrm{CHRW}}(t). \tag{29}$$

In this work, we mainly use the method based on the numerical diagonalization of $\tilde{\mathcal{H}}_{\mathrm{CHRW}}$ to study the transition probability and resonance shifts. This treatment is referred to as the CHRW method throughout this paper to distinguish it from the RWA and GFT approaches. When the longitudinal field is

sufficiently weak, we use the analytical treatment based on the Van Vleck perturbation theory.

We now show how to calculate the transient and time-average transition probabilities, which are the primary physical quantities of interest in both theory and experiment. The former is given by

$$\begin{aligned} P(t,t_0) &= |\langle +|U(t,t_0)|-\rangle|^2 \\ &= \mathrm{Tr}\{|+\rangle\langle +|U(t,t_0)|-\rangle\langle -|U^\dagger(t,t_0)\}, \end{aligned} \tag{30}$$

describing the probability of finding the qubit in the excited state $|+\rangle$ at time t when the qubit is initially in the ground state $|-\rangle$. Using Eq. (29), we can rewrite the above equation in terms of the Floquet states and quasienergies as

$$\begin{aligned} P(t,t_0) &= \mathrm{Tr}[R(t)e^{S(t)}|+\rangle\langle +|e^{-S(t)}R^\dagger(t)\tilde{U}_{\mathrm{CHRW}}(t,t_0) \\ &\quad \times R(t_0)e^{S(t_0)}|-\rangle\langle -|e^{-S(t_0)}R^\dagger(t_0)\tilde{U}^\dagger_{\mathrm{CHRW}}(t,t_0)] \\ &= \frac{1}{2} - \frac{1}{4}\sum_{i,j}\sum_{\gamma,\lambda} f_i(t)f_j(t_0)\langle\tilde{u}_\lambda(t)|\sigma_i|\tilde{u}_\gamma(t)\rangle \\ &\quad \times\langle\tilde{u}_\gamma(t_0)|\sigma_j|\tilde{u}_\lambda(t_0)\rangle e^{-i(\varepsilon_\gamma-\varepsilon_\lambda)(t-t_0)}, \end{aligned} \tag{31}$$

where $f_{i(j)}(t)$ (i or $j = x,y,z$) are given as follows:

$$f_x(t) = \sin[Z\sin(\omega_x t)]\sin(\omega_x t), \tag{32}$$

$$f_y(t) = \sin[Z\sin(\omega_x t)]\cos(\omega_x t), \tag{33}$$

$$f_z(t) = \cos[Z\sin(\omega_x t)]. \tag{34}$$

Based on this formal expression, we can readily derive the time-average transition probability

$$\begin{aligned} \overline{P} &= \overline{P(t,t_0)} \\ &= \frac{1}{2} - \frac{1}{4}\sum_\gamma \left[J_0(Z)X^{(z)}_{\gamma\gamma,0} + J_1(Z)X^{(x)}_{\gamma\gamma,0}\right]^2, \end{aligned} \tag{35}$$

where

$$X^{(i)}_{\gamma\gamma,0} = \frac{1}{T}\int_0^T \langle\tilde{u}_\gamma(t)|\sigma_i|\tilde{u}_\gamma(t)\rangle dt. \tag{36}$$

To derive the above result, one should average with respect to the time t_0 while fixing $t - t_0$ and then average over the duration $t - t_0$. It follows from Eq. (35) that the time-average transition probability is not greater than 0.5. In particular, the maximum $\overline{P} = 0.5$ indicates the resonance of the driven qubit.

III. GENERALIZED FLOQUET THEORY

To examine the validity of the CHRW and RWA Hamiltonians, we use the GFT to calculate numerically the exact transient and time-average transition probabilities of the Rabi model with modulation. The GFT states that the ansatz for the evolution operator in the case of polychromatic driving takes the form [30]

$$U(t) = \sum_\gamma |u_\gamma(t)\rangle\langle u_\gamma(0)|e^{-i\varepsilon_\gamma t}, \tag{37}$$

which is similar to the ansatz of the Floquet theory. When differentiating the above equation with respect to t, one arrives at the following equation:

$$[H(t) - i\partial_t]|u_\gamma(t)\rangle = \varepsilon_\gamma|u_\gamma(t)\rangle. \tag{38}$$

Here $|u_\gamma(t)\rangle$ is no longer periodic in time and does not possess a standard Fourier expansion. Nevertheless, it can be expanded by the "multimode" Fourier series. For $H(t)$ given in Eq. (2), we expand it by the "two-mode" Fourier series [30], which reads

$$|u_\gamma(t)\rangle = \sum_{n_x,n_z}\left|u^{(n_x,n_z)}_\gamma\right\rangle e^{i(n_x\omega_x+n_z\omega_z)t}, \tag{39}$$

where $|u^{(n_x,n_z)}_\gamma\rangle$ is a time-independent component and has the same dimension as $|u_\gamma(t)\rangle$. In addition, the Hamiltonian can be expanded similarly,

$$\begin{aligned} H(t) &= \sum_{n_x,n_z} H^{(n_x,n_z)}e^{i(n_x\omega_x+n_z\omega_z)t} \\ &= H^{(0,0)} + H^{(1,0)}e^{i\omega_x t} + H^{(-1,0)}e^{-i\omega_x t} \\ &\quad + H^{(0,1)}e^{i\omega_z t} + H^{(0,-1)}e^{-i\omega_z t}, \end{aligned} \tag{40}$$

where

$$H^{(0,0)} = \frac{\omega_0}{2}\sigma_z, \quad H^{(\pm1,0)} = \frac{\Omega_x}{2}\sigma_x, \quad H^{(0,\pm1)} = \frac{\Omega_z}{4}\sigma_z. \tag{41}$$

By substituting Eqs. (39) and (40) into Eq. (38), we readily derive the following time-independent equation:

$$\begin{aligned} &\sum_{n_x,n_z}[H^{(m_x-n_x,m_z-n_z)} + (n_x\omega_x + n_z\omega_z) \\ &\quad \times \delta_{n_x,m_x}\delta_{n_z,m_z}]\left|u^{(n_x,n_z)}_\gamma\right\rangle = \varepsilon_\gamma\left|u^{(m_x,m_z)}_\gamma\right\rangle. \end{aligned} \tag{42}$$

Similarly to Eq. (26), this equation also represents an eigenvalue equation:

$$\mathcal{H}_{F_2}|u_\gamma\rangle\rangle = \varepsilon_\gamma|u_\gamma\rangle\rangle. \tag{43}$$

Here $\mathcal{H}_{F_2}$ is the two-mode Floquet matrix and reads

$$\mathcal{H}_{F_2} = \begin{pmatrix} \ddots & \ddots & \ddots & & \\ \ddots & \mathcal{H}_F - \omega_z\mathbf{I} & \mathbf{C} & \mathbf{O} & \\ \ddots & \mathbf{C} & \mathcal{H}_F & \mathbf{C} & \ddots \\ & \mathbf{O} & \mathbf{C} & \mathcal{H}_F + \omega_z\mathbf{I} & \ddots \\ & & \ddots & \ddots & \ddots \end{pmatrix}, \tag{44}$$

where $\mathcal{H}_F$ is the single-mode Floquet matrix for a driven qubit in the absence of a longitudinal field and given by

$$\mathcal{H}_F = \begin{pmatrix} \ddots & \ddots & \ddots & & \\ \ddots & H^{(0,0)} - \omega_x\mathbf{1} & H^{(-1,0)} & \mathbf{0} & \\ \ddots & H^{(1,0)} & H^{(0,0)} & H^{(-1,0)} & \ddots \\ & \mathbf{0} & H^{(1,0)} & H^{(0,0)} + \omega_x\mathbf{1} & \ddots \\ & & \ddots & \ddots & \ddots \end{pmatrix}. \tag{45}$$

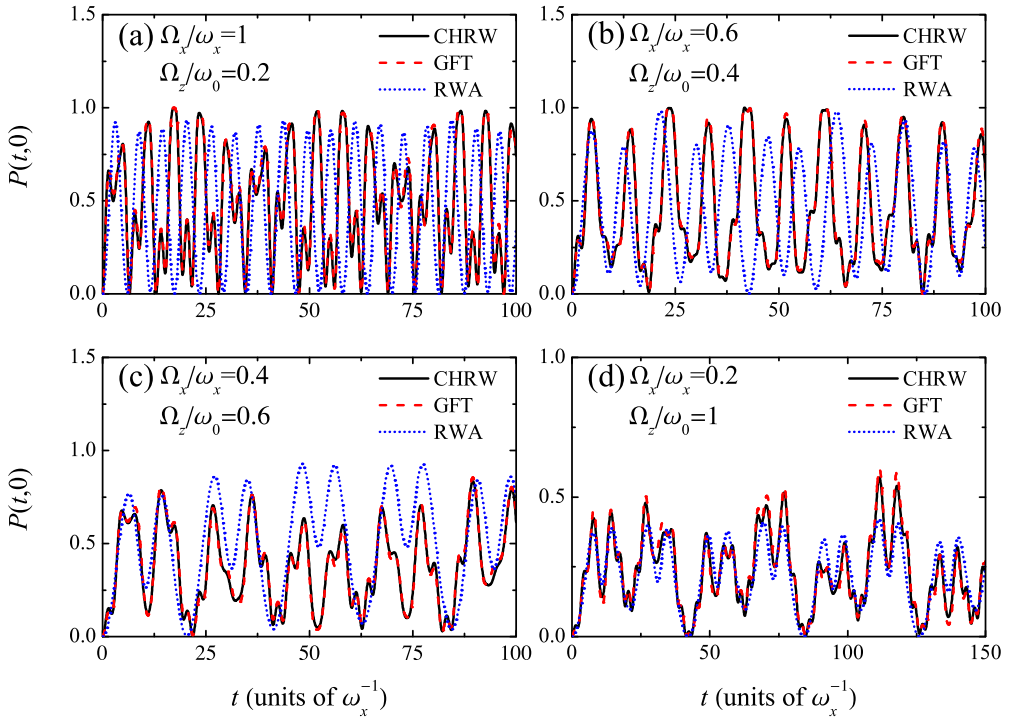

FIG. 2. Transient transition probability $P(t,0)$ versus time t for $\omega_0 = 0.6\omega_x$ and $\omega_z = 0.3\omega_x$. Other parameters are given in the plots. The CHRW and RWA results are obtained from the CHRW and RWA Hamiltonians with the Floquet theory, respectively. The GFT results are calculated from the original Hamiltonian with the generalized Floquet theory.

Here **O** and **I** represent the zero matrix and identity matrix, respectively, which have the same dimension as $\mathcal{H}_F$. **C** is an infinite-rank coupling matrix through which the diagonal blocks in $\mathcal{H}_{F_2}$ are coupled to others. Its explicit form is given by

$$\mathbf{C} = \mathrm{diag}\{\ldots, H^{(0,\pm1)}, H^{(0,\pm1)}, H^{(0,\pm1)}, \ldots\}. \tag{46}$$

The eigenstate $|u_\gamma\rangle\rangle$ is related to $|u_\gamma^{(n_x,n_z)}\rangle$ via the relation

$$\begin{aligned}|u_\gamma\rangle\rangle^{\mathrm{T}} = \big[&\ldots, \big|u_\gamma^{(-1,-1)}\big\rangle^{\mathrm{T}}, \big|u_\gamma^{(0,-1)}\big\rangle^{\mathrm{T}}, \big|u_\gamma^{(1,-1)}\big\rangle^{\mathrm{T}}, \ldots,\\ &\ldots, \big|u_\gamma^{(-1,0)}\big\rangle^{\mathrm{T}}, \big|u_\gamma^{(0,0)}\big\rangle^{\mathrm{T}}, \big|u_\gamma^{(1,0)}\big\rangle^{\mathrm{T}}, \ldots,\\ &\ldots, \big|u_\gamma^{(-1,1)}\big\rangle^{\mathrm{T}}, \big|u_\gamma^{(0,1)}\big\rangle^{\mathrm{T}}, \big|u_\gamma^{(1,1)}\big\rangle^{\mathrm{T}}, \ldots\big],\end{aligned} \tag{47}$$

where a superscript T denotes the transpose operation.

The key task of the GFT approach is to diagonalize the two-mode Floquet matrix, which is similar to the Floquet theory approach. In general, the matrix $\mathcal{H}_{F_2}$ can be numerically diagonalized with an appropriate truncation. After the diagonalization, one readily obtains its eigenstates and eigenvalues. The eigenstates can be used to construct $|u_\gamma(t)\rangle\rangle$ by using relations (39) and (47). The eigenvalues are, of course, the quasienergies. Therefore, we can obtain the evolution operator and calculate the transient and time-average transition probabilities. More details about the GFT approach can be found in the review article [30].

IV. TRANSIENT TRANSITION PROBABILITY

In this section, we examine in detail the performance of the CHRW and RWA Hamiltonians by comparing their dynamics with that of the original Hamiltonian obtained by the GFT approach. In doing so, we can get some insights into the effects of the CR terms on the dynamics as well as the accuracy of the CHRW and RWA Hamiltonians. Throughout this paper we fix the transverse frequency ω_x as the unit.

To begin with, we consider $\omega_0 = 0.6\omega_x$. In accordance with the valid regime shown in Fig. 1(a), we choose four pairs of ratios Ω_x/ω_x and Ω_z/ω_0 (which lie near the boundary of the valid regime) and set $\omega_z = 0.3\omega_x$ to carry out numerical calculation. The numerical results are shown in Fig. 2. Obviously, the CHRW results are in good agreement with the GFT results. On the contrary, the RWA results significantly deviate from the GFT results, indicating the breakdown of the RWA under strong driving conditions. In addition, Figs. 2(a) and 2(b) show that the CR terms significantly modify the Rabi oscillation frequency in the strong driving regime. Figures 2(c) and 2(d) show that for moderately strong transverse driving, the RWA cannot give accurate oscillation amplitudes even if its Rabi frequencies are similar to the exact ones of the GFT.

We move to consider $\omega_0 = \omega_x$ and choose the other parameters as in Fig. 2. We display the transient transition probability in Fig. 3. As expected, the CHRW method agrees well with the GFT approach when the driving parameters are in the valid regime. Comparing the RWA and GFT results, one readily notes that the RWA method gives a coarse-grained approximate dynamics only for $\Omega_x/\omega_x = 0.2$ [Fig. 3(d)] and breaks down for the other three values of Ω_x. It is easy to further verify that when $\omega_0 > \omega_x$, the CHRW method still

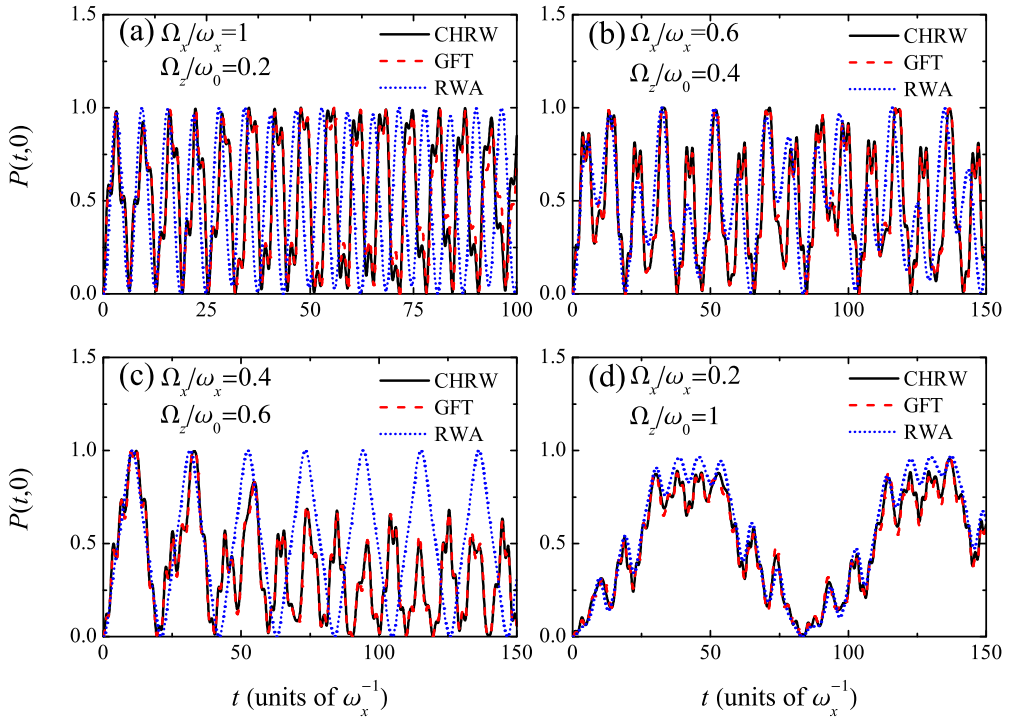

FIG. 3. Transient transition probability $P(t,0)$ versus time t for $\omega_0 = \omega_x$ and $\omega_z = 0.3\omega_x$. Other parameters are given in the plots.

holds in the valid regime even if the RWA breaks down. In comparison with the RWA and GFT results, we obtain that the CHRW Hamiltonian can still provide a correct dynamical description when the RWA Hamiltonian breaks down in the strong driving regime.

To examine whether the value of ω_z would affect the validity of the CHRW method, we carry out the numerical calculation for $\omega_0 = 0.6\omega_x$ and various ω_z values, ranging from $0.1\omega_x$ to $0.9\omega_x$, and show the results in Fig. 4. One readily finds that the dynamics of the CHRW Hamiltonian is consistent with the

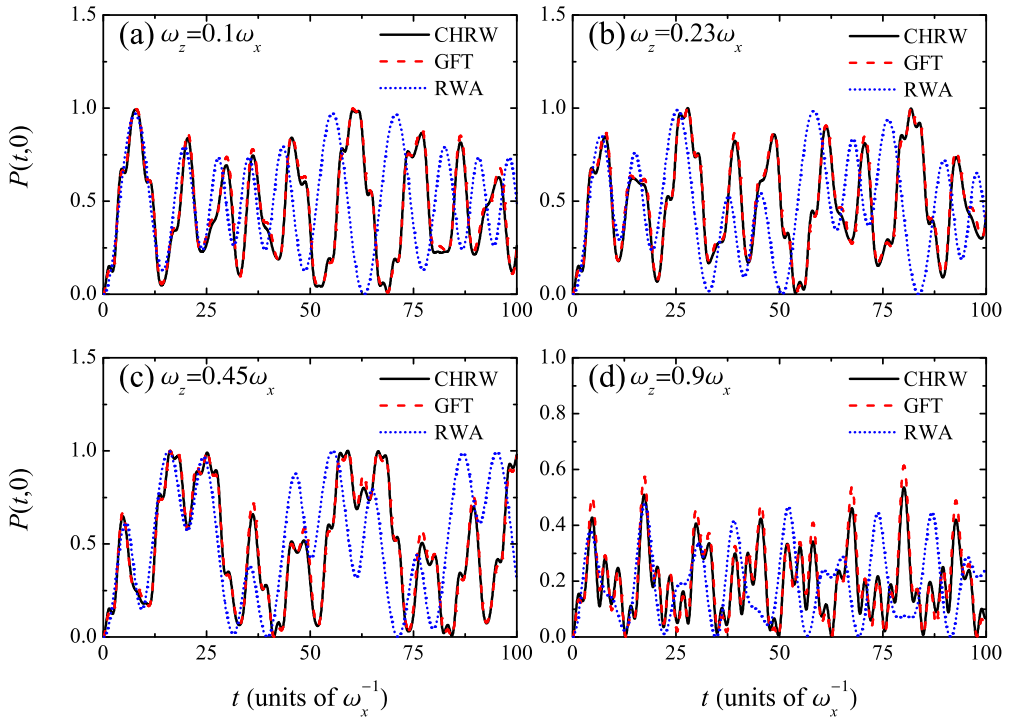

FIG. 4. Transient transition probability $P(t,0)$ versus time t for $\omega_0 = 0.6\omega_x$ and various longitudinal frequencies ω_z. Other parameters are $\Omega_x/\omega_x = 0.4$ and $\Omega_z/\omega_0 = 0.6$.

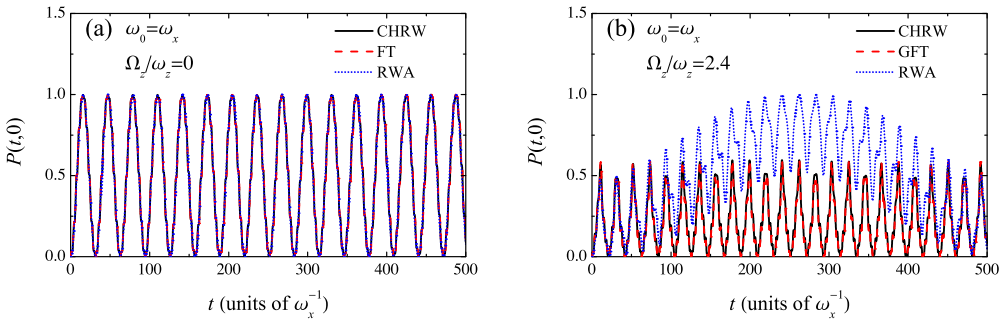

FIG. 5. Transient transition probability $P(t,0)$ versus time t for $\omega_z = 0.3\omega_x$ and $\Omega_x/\omega_x = 0.2$. Other parameters used are given in the plots.

exact dynamics of the original Hamiltonian for each ω_z, while the RWA breaks down. Nevertheless, Fig. 4 also shows that with an increase in ω_z, the difference in oscillation amplitudes between the CHRW and the GFT methods becomes larger and larger. On the other hand, when $\omega_z \geqslant \omega_x$, we find that both the CHRW and the RWA methods break down. Therefore, we conclude that the CHRW method holds in the valid regime as long as ω_z is smaller than ω_x.

To end this section, we illustrate that the longitudinal field can amplify the effects of CR coupling of the transverse field in a moderately strong transverse driving regime, e.g., $\Omega_x/\omega_x = 0.2$. In Figs. 5(a) and 5(b), we show the dynamics of the driven qubit for $\Omega_z/\omega_z = 0$ and $\Omega_z/\omega_z = 2.4$, respectively. The other parameters are given by $\omega_0 = \omega_x$ and $\omega_z = 0.3\omega_x$. Obviously, one notes that the RWA, CHRW, and Floquet theory results are in good agreement with each other without modulation ($\Omega_z/\omega_z = 0$). However, the RWA result becomes dramatically different from the CHRW and GFT results for $\Omega_z/\omega_z = 2.4$, indicating that the longitudinal field can intensify the effects of the CR terms on the dynamics under certain conditions. In Figs. 6(a) and 6(b), we plot the dynamics of the driven qubit for $\Omega_z/\omega_z = 0$ and $\Omega_z/\omega_z = 0.05$, respectively, with $\omega_0 = 0.7127\omega_x$ [this value of ω_0 corresponds to the maximum position of the RWA curve in Fig. 10(d)] and $\omega_z = 0.35\omega_x$. Similarly, the difference between the RWA and the other non-RWA results becomes larger in the case of $\Omega_z/\omega_z = 0.05$ than in the case of $\Omega_z/\omega_z = 0$. These results lead us to conclude that the application of a longitudinal field can intensify the effects of the CR terms under certain conditions. In what follows, we carry out a comprehensive study to clarify how the effects of the CR terms are heightened with modulation of the longitudinal field.

V. TIME-AVERAGE TRANSITION PROBABILITY AND BLOCH-SIEGERT SHIFTS

In this section, first we illustrate how the CR terms of a transverse field modify the resonance curves of a bichromatically driven qubit. Then we analyze the effects of longitudinal modulation on the resonance curves to demonstrate how the effects of the CR terms of the transverse field can be amplified. We discuss in detail how the resonance shifts at the central band and sideband due to the CR terms of the transverse field and the modulation of the longitudinal field.

In Fig. 7, we plot the time-average transition probability as a function of ω_0 for a fixed ratio $\Omega_x/\omega_x = 0.2$ and four different ratios Ω_z/ω_z. In all plots, the CHRW results are found to be almost indistinguishable from the numerically exact results except for some ultranarrow peaks, which are generally too narrow to be observed. The ultranarrow peaks can be safely neglected in most cases except that when the ratio Ω_z/ω_z is large enough, some of them may possess nonvanishing width as shown in the inset in Fig. 7(d). The additional narrow peaks correspond to multiphoton resonances at $\omega_0 \approx n\omega_x + m\omega_z$ for $n > 1$ and $m \neq 0$ and are not taken into account by the CHRW Hamiltonian due to the neglect of $\tilde{H}_2(t)$. We concentrate on the resonance at $\omega_0 \approx \omega_x + m\omega_z$ in the present paper and discuss other multiphoton resonances elsewhere. By comparing the CHRW and GFT results with the RWA results, one readily figures out the modifications to the time-average transition probability resulting from the CR terms of the transverse field. First, the RWA curves are symmetric about the center $\omega_0 = \omega_x$. However, the CHRW and GFT curves are not symmetric with respect to the center, indicating that the CR terms lift the symmetry. Second, there are shifts between the curves of the RWA and those of the non-RWA theories. Needless to say, the shifts

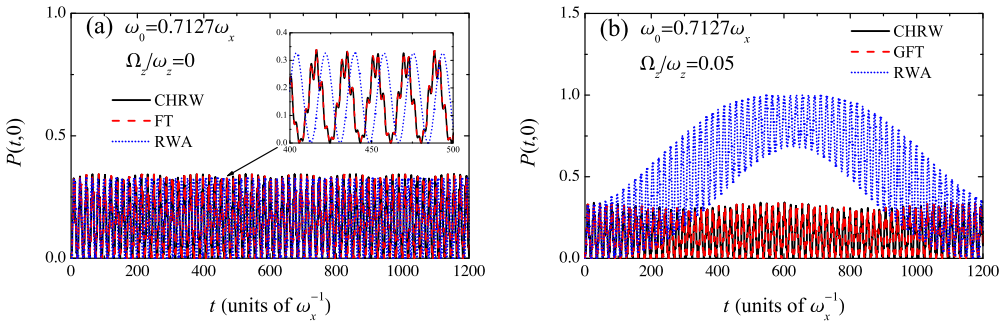

FIG. 6. Transient transition probability $P(t,0)$ versus time t for $\omega_z = 0.35\omega_x$ and $\Omega_x/\omega_x = 0.2$. Other parameters used are given in the plots. Inset in (a): Dynamics at the time interval $(400, 500)\omega_x^{-1}$.

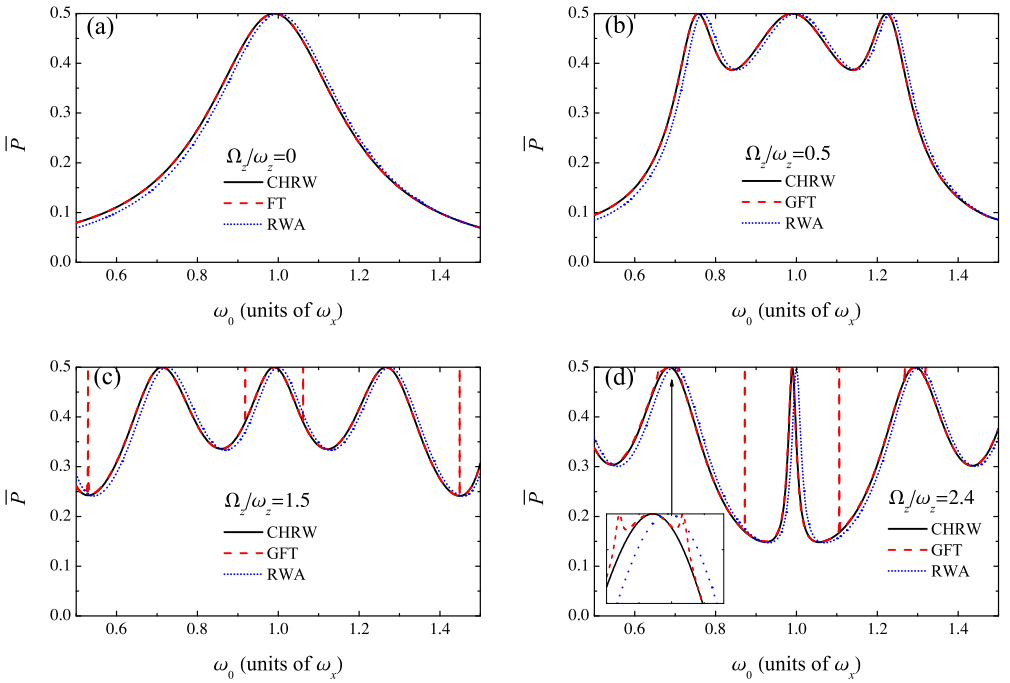

FIG. 7. Time-average transition probability $\overline{P}$ versus ω_0 for $\Omega_x = 0.2\omega_x$, $\omega_z = 0.3\omega_x$, and various ratios Ω_z/ω_z. Inset in (d): The three resonance peaks near $0.7\omega_x$.

are actually the BS shifts caused by the CR terms, which are neglected within the framework of the RWA. The present results show that the BS shifts can be observed not only at the central band peaking at $\omega_0 \approx \omega_x$ but also at the sidebands peaking at $\omega_0 \approx \omega_x + m\omega_z$. We discuss the BS shifts in detail later.

To clarify how the longitudinal field heightens the difference between the RWA and the non-RWA theories as shown in Figs. 5(b) and 6(b), we analyze the roles of longitudinal modulation on the time-average transition probability shown in Fig. 7. We first focus on the central bands in Fig. 7. As the ratio Ω_z/ω_z increases, the width of the central peak significantly decreases. In particular, when $\Omega_z/\omega_z = 2.4$, the width of the central peak becomes comparable to the magnitude of the BS shift. As a consequence, the resonance position $\omega_0 = \omega_x$ of the RWA Hamiltonian actually becomes an off-resonance position far from the resonance of the non-RWA Hamiltonian, i.e., the BS shift cannot be neglected, which results in the significant dynamical difference between the RWA and the non-RWA results shown in Fig. 5(b). In contrast, when $\Omega_z = 0$, one can see that the resonance width is much larger than the BS shift, and the RWA resonance position, i.e., $\omega_0 = \omega_x$, is close to the resonance position for the non-RWA Hamiltonian. Thus, the BS shift is negligible. It follows that the RWA prediction is consistent with those of the non-RWA Hamiltonians as shown in Fig. 5(a). In the same way, the difference between the RWA and the non-RWA theories shown in Fig. 6(b) can be understood using a similar analysis based on the RWA and non-RWA resonance curves shown in Fig. 10(d). The present results show that under certain conditions, the resonance width can be modified by longitudinal modulation to be comparable to the BS shift. In contrast, this phenomenon hardly occurs for the Rabi model without longitudinal modulation in a moderately strong driving regime due to power broadening. As a consequence, when the transverse field is moderately strong, the CR-induced BS shift becomes more important in the Rabi model with longitudinal modulation than in that without longitudinal modulation, indicating that the effect of the CR terms is heightened.

It is well known that power broadening adversely affects the measurement of the BS shift in the Rabi model [33]. The present results indicate that longitudinal modulation may help to remove this inevitable adverse effect. We briefly discuss conditions under which the widths of resonance peaks can be narrowed by longitudinal modulation. By numerical simulation of the transition probability, it is found that the width of the central peak becomes significantly small when ω_z is much larger than Ω_x and Ω_z/ω_z is large enough. In contrast with the central band, the small widths of the sidebands are easily obtained with a relatively weak longitudinal modulation ($\Omega_z/\omega_z \ll 1$) as long as ω_z is much larger than Ω_x. In what follows, we examine the combined effects of the longitudinal field and CR terms on the resonance positions.

A. Central-band Bloch-Siegert shifts

In Fig. 8, we plot the resonance positions at the central band as a function of Ω_x for $\omega_z = 0.3\omega_x$ and $\Omega_z/\omega_z = 2$. The resonance positions are obtained by numerically searching the positions of the maximum $\overline{P} = 0.5$, denoted $\omega_{\rm res}$. It is evident that the CHRW and GFT approaches are consistent with each other, i.e., they predict that the larger the transverse field strength Ω_x is, the smaller the resonance position $\omega_{\rm res}$ becomes. In contrast, the RWA resonance position is independent of Ω_x and remains at $\omega_{\rm res} = \omega_x$. In addition, one finds that there is a slight deviation between the CHRW and the GFT results, implying that the CHRW method slightly underestimates the BS shift because of the neglect of $\tilde{H}_2(t)$. Nevertheless, the devi-

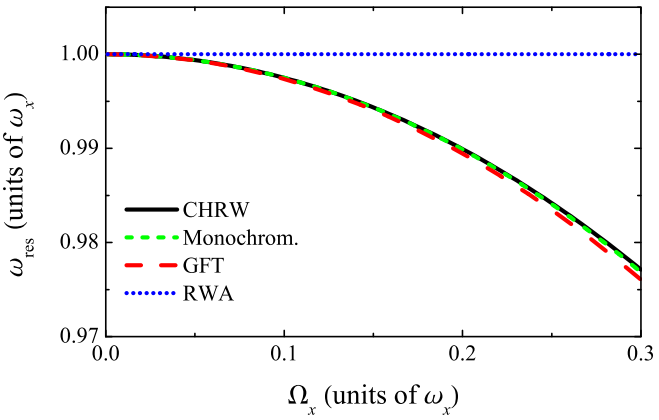

FIG. 8. The resonance position $\omega_{\rm res}$ of the central band near ω_x for $\omega_z = 0.3\omega_x$ and $\Omega_z/\omega_z = 2$. The "monochrom." curve represents the positions of the main resonance of the monochromatically driven qubit when $\Omega_z = 0$, which is obtained by the Floquet theory.

ation is very small and negligible compared to the BS shift (the gap between the dashed line and the solid line is very small).

Next we analyze the effects of longitudinal modulation on the central-band BS shift. Figure 8 shows that the CHRW curve (solid line) is almost indistinguishable from the curve for the monochromatically driven qubit (short-dashed line). The value of $\omega_{\rm res}$ given in the CHRW and monochromatic cases, respectively, is slightly larger than that of the GFT for a fixed Ω_x. This indicates that longitudinal modulation is able to enhance slightly the central-band BS shift under certain conditions. To further investigate this effect, in Fig. 9(a), we plot the central-band BS shift for a fixed ratio $\Omega_z/\omega_z = 2$ and three ω_z values by using the exact GFT approach. The resonance positions are found to shift towards smaller values with increasing ω_z when Ω_z/ω_z is fixed. In Fig. 9(b), we display the dependence of the BS shift on Ω_x for a given ω_z

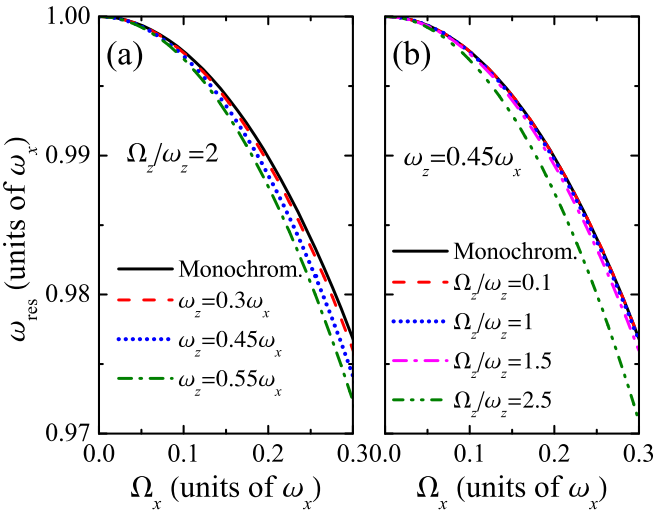

FIG. 9. (a) Resonance positions of the central band for various longitudinal frequencies and the fixed ratio $\Omega_z/\omega_z = 2$. (b) Resonance positions of the central band for various ratios Ω_z/ω_z and a fixed $\omega_z = 0.45\omega_x$. All curves but the "monochrom." ones are obtained by the GFT approach.

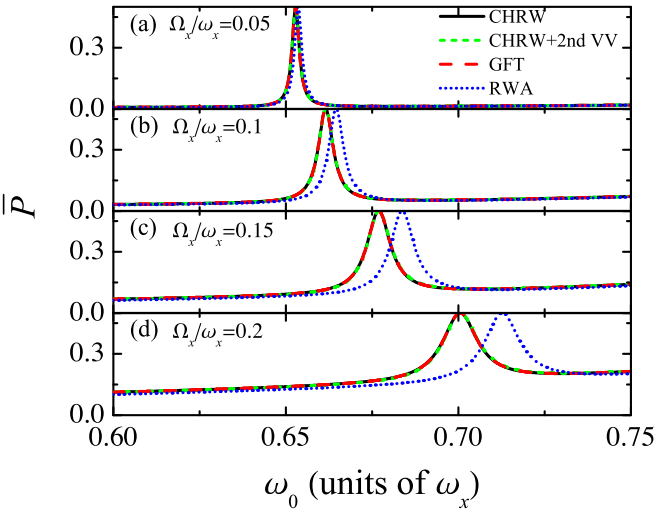

FIG. 10. Time-average transition probability $\overline{P}$ versus ω_0 for $\omega_z = 0.35\omega_x$, $\Omega_z/\omega_z = 0.05$, and four driving strengths Ω_x. The CHRW result is obtained based on the numerical diagonalization of the Floquet Hamiltonian. The CHRW + 2nd VV results are calculated based on the effective Rabi frequency given by the second Van Vleck perturbation theory.

and different ratios Ω_z/ω_z, calculated by the GFT method. It turns out that the higher the ratio is, the larger the BS shift becomes (the gap between the curve and the horizontal line $\omega_{\rm res} = \omega_x$ becomes larger). Nevertheless, when $\Omega_z/\omega_z \leqslant 1$, the increase in the BS shift is generally negligible. Even at $1 < \Omega_z/\omega_z \leqslant 2.5$ ($0.45 < \Omega_z/\omega_x \leqslant 1.125$ is a very high strength), the increment in the BS shift is also much smaller than the magnitudes of the BS shift. Therefore, even though the CHRW Hamiltonian fails to capture the effect that longitudinal modulation can slightly enhance the central-band BS shift [due to the neglect of $\tilde{H}_2(t)$], it still provides reasonable results compared to the GFT in the valid regime.

B. Sideband Bloch-Siegert shifts

To show explicitly the shift of the sidebands, Figs. 10(a)–10(d) show the time-average transition probability close to $0.65\omega_x$ for $\omega_z = 0.35\omega_x$, $\Omega_z/\omega_z = 0.05$, and four Ω_x values. As Ω_x increases, it is clearly shown that the resonance peaks of both the RWA and the non-RWA Hamiltonians shift towards a larger ω_0. For the RWA Hamiltonian, the shift from the position at $\omega_0 = \omega_x - \omega_z$ can be completely attributed to the fast-oscillating terms of the longitudinal modulation, which can be analytically characterized by the theory given in Ref. [26]. We call this type of shift $\delta_{\rm d}$ shift. For the CHRW and original Hamiltonians, it turns out that the shift from $0.65\omega_x$ is smaller than the RWA one at a given Ω_x. There are shifts between the RWA and non-RWA peaks, which also increases with Ω_x. Needless to say, this is the BS shift caused by the CR terms of the transverse field. Therefore, the sidebands generally have two types of resonance shifts: $\delta_{\rm d}$ shift and BS shift. More importantly, Fig. 10 shows that the width of the sideband can be comparable to the magnitude of the BS shift, leading to the essential effect of the CR terms in the bichromatically driven qubit as mentioned.

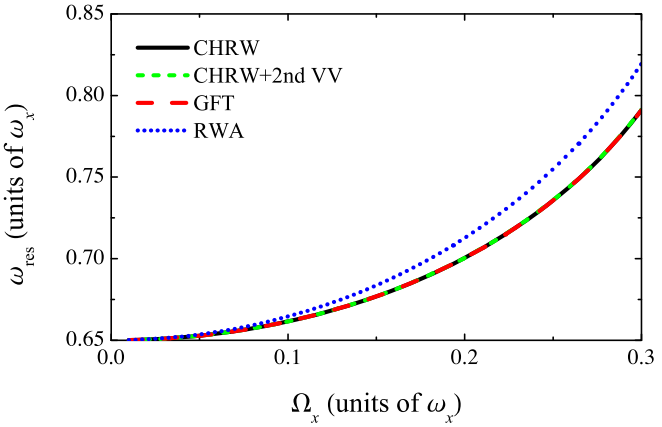

FIG. 11. Resonance position $\omega_{\rm res}$ of the sideband near $\omega_x - \omega_z$ for $\omega_z = 0.35\omega_x$ and $\Omega_z/\omega_z = 0.05$.

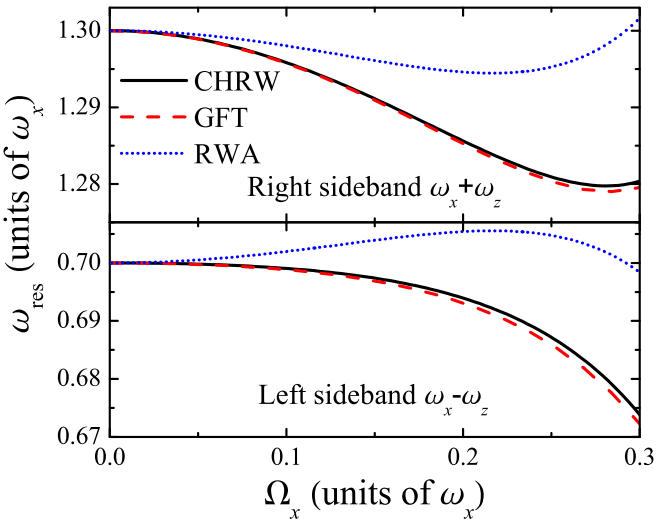

FIG. 12. Resonance positions $\omega_{\rm res}$ of the sidebands near $\omega_x \pm \omega_z$ for $\omega_z = 0.3\omega_x$ and $\Omega_z/\omega_z = 2$.

When $\Omega_z/\omega_z \ll 1$, we find that it is convenient to analytically calculate the time-average transition probability by the effective Rabi frequency $W_{\rm R}$ given in (A25), derived from the effective Hamiltonian. We present the analytical derivation of the effective Rabi frequency by the Van Vleck perturbation theory in Appendix A. Figure 10 shows that the analytical results are in excellent agreement with those of the numerical approaches, indicating that the analytical treatment is capable of giving a correct description in the limit case. In addition, it provides an alternative way to calculate the resonance positions, i.e., one can obtain the resonance frequency by solving the equation $\frac{\partial W_{\rm R}}{\partial \omega_0} = 0$ for the variable ω_0. Below we study the behavior of the resonance positions as Ω_x increases and compare results from the analytical treatment and the numerical approaches.

In Fig. 11, we plot the behaviors of the resonance position of the sideband near $0.65\omega_x$ with the variation of Ω_x for the same ω_z and Ω_z/ω_z as given in Fig. 10. Except for the CHRW + 2nd VV curve, the other curves are obtained by numerically searching the maximum position of the time-average transition probability near $0.65\omega_x$. The dotted line shows that when $\Omega_z/\omega_z \ll 1$, the $\delta_{\rm d}$ shift monotonously increases as Ω_x increases. Moreover, one finds that the gap between the RWA curve and the horizontal axis is much larger than the gap between the RWA and the non-RWA curves. In other words, the magnitude of the $\delta_{\rm d}$ shift is larger than that of the BS shift. Nevertheless, this does not mean that the BS shift is not important in this scenario. As mentioned above, the width of the sideband is comparable to the magnitude of the BS shift, leading to the breakdown of the RWA theory. Comparing the numerical results for the perturbation theory with the exact ones, one finds excellent agreement between them, indicating that when $\Omega_z/\omega_z \ll 1$ the resonance positions for the bichromatically driven qubit can be directly calculated from $\frac{\partial W_{\rm R}}{\partial \omega_0} = 0$.

In general, the behaviors of resonance positions at sidebands with the variation of Ω_x are generally more complex than those at the central band and strongly depend on the longitudinal field parameters. We consider a relatively strong longitudinal field. Figure 12 displays the dependence of the sideband resonance positions on Ω_x for $\omega_z = 0.3\omega_x$ and $\Omega_z/\omega_z = 2$. It is clear that the RWA sideband resonance position nonmonotonously varies with Ω_x. In addition, the gap between the RWA curve and the line $\omega_{\rm res} = \omega_x + m\omega_z$ ($m = \pm 1$ in this case) is smaller than the gap between the RWA and the CHRW (GFT) curves, i.e., the absolute value of the $\delta_{\rm d}$ shift is smaller than that of the BS shift. This is in contrast with the case of the weak longitudinal field shown in Fig. 11.

VI. CONCLUSIONS

In summary, we have systematically studied the dynamics and BS shifts of the Rabi model with frequency modulation. Based on the unitary transformation, we have derived an effective periodic Hamiltonian, the evolution operator of which can be obtained by the efficient Floquet theory approach. We carefully examined the performance of the effective Hamiltonian and the RWA Hamiltonian in the strong driving regime. It was found that over a wide range of parameters, the effective Hamiltonian can provide a much more accurate description than the RWA Hamiltonian compared to the results with the original Hamiltonian obtained by the exact GFT approach. We found that under certain conditions, longitudinal modulation can heighten the effects of the CR terms on the dynamics, leading to the breakdown of the RWA in the Rabi model with frequency modulation, although it holds in the Rabi model without modulation. This follows from the fact that the longitudinal field can significantly reduce the resonance width to the magnitude of the BS shift, and as a result, the BS shifts become essentially important and the RWA and non-RWA dynamics becomes dramatically different at the resonance positions given by the RWA.

By using the effective Hamiltonian, we can use both analytical and numerical methods to calculate the time-average transition probability and evaluate the resonance positions at $\omega_0 \approx \omega_x + m\omega_z$ for a bichromatically driven qubit, which are in good agreement with the exact resonance positions derived with the original Hamiltonian. More importantly, the CHRW method is more efficient in numerical calculation than the GFT

approach, which requires significant cost for higher precision. In the case of weak longitudinal modulation, we have shown that the effective Rabi frequency for a doubly dressed qubit can be used to calculate the time-average transition probability and resonance positions, which are in excellent agreement with the exact numerical results. Our results indicate that the resonance shifts of the sidebands may be experimentally accessed with weak longitudinal modulation and moderately strong transverse excitation. More importantly, power broadening can be significantly suppressed in the bichromatically driven qubit, which is conducive to the experimental measurement of resonance shifts.

ACKNOWLEDGMENTS

This work was supported by the National Natural Science Foundation of China (Grants No. 11474200, No. 11374208, No. 11647082, and No. 11774226).

APPENDIX A: VAN VLECK PERTURBATION CALCULATION OF THE EFFECTIVE RABI FREQUENCY

To calculate the effective Rabi frequency for the effective Hamiltonian, we introduce a set of new spin-1/2 operators, i.e., dressed operators,

$$\begin{pmatrix} s_x \\ s_y \\ s_z \end{pmatrix} = \frac{1}{\tilde{\Omega}_{\mathrm{R}}} \begin{pmatrix} \tilde{\delta} & 0 & -\tilde{\Omega}_x \\ 0 & \tilde{\Omega}_{\mathrm{R}} & 0 \\ \tilde{\Omega}_x & 0 & \tilde{\delta} \end{pmatrix} \begin{pmatrix} \sigma_x \\ \sigma_y \\ \sigma_z \end{pmatrix}, \tag{A1}$$

where

$$\tilde{\delta} = J_0(Z)\omega_0 - \omega_x \tag{A2}$$

is the effective detuning, and

$$\tilde{\Omega}_{\mathrm{R}} = \sqrt{\tilde{\delta}^2 + \tilde{\Omega}_x^2} \tag{A3}$$

is the effective Rabi frequency of the qubit merely dressed by the transverse field. The effective Hamiltonian can be rewritten as

$$\tilde{H}_{\mathrm{CHRW}}(t) = \tfrac{1}{2}\tilde{\Omega}_{\mathrm{R}} s_z + \tfrac{1}{2}\Omega_z \cos(\omega_z t)(g s_x + f s_z), \tag{A4}$$

where

$$g = J_1(Z)\frac{\tilde{\delta}}{\tilde{\Omega}_{\mathrm{R}}} - J_0(Z)\frac{\tilde{\Omega}_x}{\tilde{\Omega}_{\mathrm{R}}}, \tag{A5}$$

$$f = J_0(Z)\frac{\tilde{\delta}}{\tilde{\Omega}_{\mathrm{R}}} + J_1(Z)\frac{\tilde{\Omega}_x}{\tilde{\Omega}_{\mathrm{R}}}. \tag{A6}$$

We further transform the Hamiltonian with the generator

$$X(t) = i\frac{\Omega_z}{2\omega_z} f \sin(\omega_z t) s_z, \tag{A7}$$

yielding

$$\begin{aligned} \tilde{H}'_{\mathrm{CHRW}}(t) &= e^{X(t)}[\tilde{H}_{\mathrm{CHRW}}(t) - i\partial_t]e^{-X(t)} \\ &= \frac{1}{2}\tilde{\Omega}_{\mathrm{R}} s_z + \sum_l (p_l s_+ + p_{-l} s_-) e^{il\omega_z t}, \end{aligned} \tag{A8}$$

with

$$p_l = \frac{1}{4}\Omega_z g\left[J_{l-1}\left(\frac{\Omega_z}{\omega_z} f\right) + J_{l+1}\left(\frac{\Omega_z}{\omega_z} f\right)\right], \tag{A9}$$

$$s_\pm = (s_x \pm i s_y)/2. \tag{A10}$$

The resulting transformed Hamiltonian is still periodic in time and its Rabi frequency can be derived by Floquet theory. Employing the product basis $|\tilde{\uparrow}(\tilde{\downarrow}),n\rangle \equiv |\tilde{\uparrow}(\tilde{\downarrow})\rangle \otimes |n\rangle$ with $s_z|\tilde{\uparrow}(\tilde{\downarrow})\rangle = +(-)|\tilde{\uparrow}(\tilde{\downarrow})\rangle$ and $|n\rangle \equiv \exp(in\omega_z t)$ $(n = 0, \pm1, \pm2, \dots)$ and the inner product $\langle n|m\rangle = \frac{1}{T}\int_0^T \exp[-i(n-m)\omega_z t]dt$, the Floquet Hamiltonian $\tilde{\mathcal{H}}'_{\mathrm{CHRW}} = \tilde{H}'_{\mathrm{CHRW}}(t) - i\partial_t$ reads

$$\tilde{\mathcal{H}}'_{\mathrm{CHRW}} = \left(\begin{array}{c|cccccc|c} \ddots & |\tilde{\uparrow},n-1\rangle & |\tilde{\downarrow},n-1\rangle & |\tilde{\uparrow},n\rangle & |\tilde{\downarrow},n\rangle & |\tilde{\uparrow},n+1\rangle & |\tilde{\downarrow},n+1\rangle & \\ \hline |\tilde{\uparrow},n-1\rangle & E_{\tilde{\uparrow},n-1} & 0 & 0 & p_{-1} & 0 & p_{-2} & \\ |\tilde{\downarrow},n-1\rangle & 0 & E_{\tilde{\downarrow},n-1} & p_1 & 0 & p_2 & 0 & \\ |\tilde{\uparrow},n\rangle & 0 & p_1 & E_{\tilde{\uparrow},n} & 0 & 0 & p_{-1} & \\ |\tilde{\downarrow},n\rangle & p_{-1} & 0 & 0 & E_{\tilde{\downarrow},n} & p_1 & 0 & \\ |\tilde{\uparrow},n+1\rangle & 0 & p_2 & 0 & p_1 & E_{\tilde{\uparrow},n+1} & 0 & \\ |\tilde{\downarrow},n+1\rangle & p_{-2} & 0 & p_{-1} & 0 & 0 & E_{\tilde{\downarrow},n+1} & \\ \hline & & & & & & & \ddots \end{array}\right), \tag{A11}$$

where

$$E_{\tilde{\uparrow},n} = \tfrac{1}{2}\tilde{\Omega}_{\mathrm{R}} + n\omega_z, \tag{A12}$$

$$E_{\tilde{\downarrow},n} = -\tfrac{1}{2}\tilde{\Omega}_{\mathrm{R}} + n\omega_z. \tag{A13}$$

To proceed, we use the Van Vleck perturbation theory to calculate the eigenvalues for $\tilde{\mathcal{H}}'_{\mathrm{CHRW}}$. The Floquet Hamiltonian can be divided into two parts. One is the diagonal part, which is treated as the free Hamiltonian H_0. The other is the off-diagonal part treated as the perturbation V. The two degenerate states can be constructed by the condition

$$E_{\tilde{\uparrow},n-m} \approx E_{\tilde{\downarrow},n} \tag{A14}$$

or, alternatively,

$$\tilde{\Omega}_{\mathrm{R}} \approx m\omega_z, \tag{A15}$$

where m is an integer nearest to $\tilde{\Omega}_{\mathrm{R}}/\omega_z$. By this construction, we have the projection operator on the subspace spanned by two degenerate states

$$\Pi_n = |\tilde{\uparrow},n-m\rangle\langle\tilde{\uparrow},n-m| + |\tilde{\downarrow},n\rangle\langle\tilde{\downarrow},n|. \tag{A16}$$

We use a further unitary transformation to transform the Floquet Hamiltonian into a block diagonal matrix accurate up to a certain order in the perturbation [4,34]. Using

$$e^{iK}Ae^{-iK} = A + [iK,A] + \frac{1}{2!}[iK,[iK,A]] + \cdots$$

and the series expansion of the generator in the perturbation (superscripts indicate orders),

$$iK = iK^{(1)} + iK^{(2)} + iK^{(3)} + \cdots,$$

we have the transformed Floquet Hamiltonian up to second order in the perturbation

$$\tilde{\mathcal{H}}''_{\mathrm{CHRW}} = H_0 + V + [iK^{(1)},H_0] + [iK^{(1)},V] + [iK^{(2)},H_0] + \tfrac{1}{2}[iK^{(1)},[iK^{(1)},H_0]] + \cdots. \tag{A17}$$

$\tilde{\mathcal{H}}''_{\mathrm{CHRW}}$ becomes a block diagonal matrix if

$$\Pi_n \tilde{\mathcal{H}}''_{\mathrm{CHRW}} \Pi_l = 0 \tag{A18}$$

with $n \neq l$. A further assumption,

$$\Pi_n K \Pi_n = 0, \tag{A19}$$

is imposed on K such that it does not have matrix elements inside each subspace of two degenerate states. Under these conditions, the generator can be determined order by order. For Eq. (A11), one readily finds that the nonvanishing elements of K up to first order are given by

$$\langle\tilde{\uparrow},n|iK^{(1)}|\tilde{\downarrow},l\rangle = \frac{p_{n-l}}{\tilde{\Omega}_{\mathrm{R}} + (n-l)\omega_z}, \tag{A20}$$

$$\langle\tilde{\downarrow},l|iK^{(1)}|\tilde{\uparrow},n\rangle = -\frac{p_{n-l}}{\tilde{\Omega}_{\mathrm{R}} + (n-l)\omega_z} \tag{A21}$$

for $n - l \neq -m$. Then the nonvanishing diagonal blocks of the Floquet Hamiltonian up to second order in the perturbation can be calculated by [4,34]

$$\tilde{\mathcal{H}}''^{(n)}_{\mathrm{CHRW}} = H_0\Pi_n + \Pi_n V \Pi_n + \frac{1}{2}\Pi_n[iK^{(1)},V]\Pi_n = \begin{pmatrix} E_{\tilde{\uparrow},n-m} + \sum_{l\neq -m}\frac{p_l^2}{\tilde{\Omega}_{\mathrm{R}}+l\omega_z} & p_{-m} \\ p_{-m} & E_{\tilde{\downarrow},n} - \sum_{l\neq -m}\frac{p_l^2}{\tilde{\Omega}_{\mathrm{R}}+l\omega_z} \end{pmatrix}. \tag{A22}$$

Its eigenenergies are given by

$$\lambda_{\tilde{\uparrow},n-m} = n\omega_z - \tfrac{1}{2}m\omega_z + \tfrac{1}{2}W_{\mathrm{R}}, \tag{A23}$$

$$\lambda_{\tilde{\downarrow},n} = n\omega_z - \tfrac{1}{2}m\omega_z - \tfrac{1}{2}W_{\mathrm{R}}, \tag{A24}$$

where

$$W_{\mathrm{R}} = \sqrt{\left(m\omega_z - \tilde{\Omega}_{\mathrm{R}} - 2\sum_{l\neq -m}\frac{p_l^2}{\tilde{\Omega}_{\mathrm{R}}+l\omega_z}\right)^2 + 4p_{-m}^2} \tag{A25}$$

is the effective Rabi frequency of the doubly dressed qubit. It is straightforward to verify that the effective Rabi frequency is related to the quasienergies of the original Hamiltonian via $\varepsilon_{\pm,k,l} = (\omega_x - m\omega_z \pm W_R)/2 + k\omega_x + l\omega_z$ for k and l any integer. On the other hand, recall that the time-average transition probability can be calculated by the derivative of the quasienergy with respect to ω_0 [13],

$$\overline{P} = \frac{1}{2}\left[1 - 4\left(\frac{\partial\varepsilon}{\partial\omega_0}\right)^2\right],$$

leading to

$$\overline{P} = \frac{1}{2}\left[1 - \left(\frac{\partial W_{\mathrm{R}}}{\partial\omega_0}\right)^2\right]. \tag{A26}$$

This means that we can directly calculate the time-average transition probability via the derivative of the effective Rabi frequency with respect to ω_0.

APPENDIX B: DERIVATIVE OF THE EFFECTIVE RABI FREQUENCY

To determine the time-average transition probability, we derive the derivative of the effective Rabi frequency with respect to ω_0. It can be calculated straightforwardly:

$$\frac{\partial W_{\mathrm{R}}}{\partial\omega_0} = \frac{1}{W_{\mathrm{R}}}\left\{\left(m\omega_z - \tilde{\Omega}_{\mathrm{R}} - 2\sum_{l\neq -m}\frac{p_l^2}{\tilde{\Omega}_{\mathrm{R}}+l\omega_z}\right) \times\left[\left(2\sum_{l\neq -m}\frac{p_l^2}{(\tilde{\Omega}_{\mathrm{R}}+l\omega_z)^2} - 1\right)\frac{\partial\tilde{\Omega}_{\mathrm{R}}}{\partial\omega_0} - 4\sum_{l\neq -m}\frac{p_l}{\tilde{\Omega}_{\mathrm{R}}+l\omega_z}\frac{\partial p_l}{\partial\omega_0}\right] + 4p_{-m}\frac{\partial p_{-m}}{\partial\omega_0}\right\}, \tag{B1}$$

which can be fully determined by the derivatives

$$\frac{\partial p_l}{\partial\omega_0} = \frac{1}{4}\Omega_z\left[J_{l-1}\left(\frac{\Omega_z}{\omega_z}f\right) + J_{l+1}\left(\frac{\Omega_z}{\omega_z}f\right)\right]\frac{\partial g}{\partial\omega_0} + \frac{1}{8}\Omega_z g\left[J_{l-2}\left(\frac{\Omega_z}{\omega_z}f\right) - J_{l+2}\left(\frac{\Omega_z}{\omega_z}f\right)\right]\frac{\partial f}{\partial\omega_0}, \tag{B2}$$

$$\frac{\partial g}{\partial\omega_0} = \left\{[J_0(Z) - J_2(Z)]\frac{\tilde{\delta}}{\tilde{\Omega}_{\mathrm{R}}} + 2J_1(Z)\frac{\tilde{\Omega}_x}{\tilde{\Omega}_{\mathrm{R}}}\right\}\frac{\Omega_x}{\omega_x}\frac{\partial\xi}{\partial\omega_0} - J_0(Z)\left(\frac{\partial\tilde{\Omega}_x}{\partial\omega_0} - \frac{\tilde{\Omega}_x}{\tilde{\Omega}_{\mathrm{R}}^2}\frac{\partial\tilde{\Omega}_{\mathrm{R}}}{\partial\omega_0}\right) + J_1(Z)\left(\frac{\partial\tilde{\delta}}{\partial\omega_0} - \frac{\tilde{\delta}}{\tilde{\Omega}_{\mathrm{R}}^2}\frac{\partial\tilde{\Omega}_{\mathrm{R}}}{\partial\omega_0}\right), \tag{B3}$$

$$\frac{\partial f}{\partial \omega_0} = \left\{ [J_0(Z) - J_2(Z)]\frac{\tilde{\Omega}_x}{\tilde{\Omega}_R} - 2J_1(Z)\frac{\tilde{\delta}}{\tilde{\Omega}_R} \right\} \frac{\Omega_x}{\omega_x}\frac{\partial \xi}{\partial \omega_0} + J_0(Z)\left(\frac{\partial \tilde{\delta}}{\partial \omega_0} - \frac{\tilde{\delta}}{\tilde{\Omega}_R^2}\frac{\partial \tilde{\Omega}_R}{\partial \omega_0} \right) + J_1(Z)\left(\frac{\partial \tilde{\Omega}_x}{\partial \omega_0} - \frac{\tilde{\Omega}_x}{\tilde{\Omega}_R^2}\frac{\partial \tilde{\Omega}_R}{\partial \omega_0} \right), \tag{B4}$$

$$\frac{\partial \tilde{\Omega}_R}{\partial \omega_0} = \frac{1}{\tilde{\Omega}_R}\left[\tilde{\delta}\frac{\partial \tilde{\delta}}{\partial \omega_0} + \tilde{\Omega}_x\frac{\partial \tilde{\Omega}_x}{\partial \omega_0} \right], \tag{B5}$$

$$\frac{\partial \tilde{\delta}}{\partial \omega_0} = J_0(Z) - 2\omega_0 J_1(Z)\frac{\Omega_x}{\omega_x}\frac{\partial \xi}{\partial \omega_0}, \tag{B6}$$

$$\frac{\partial \tilde{\Omega}_x}{\partial \omega_0} = -2\Omega_x\frac{\partial \xi}{\partial \omega_0}, \tag{B7}$$

and

$$\frac{\partial \xi}{\partial \omega_0} = -\frac{\omega_x}{(\omega_0+\omega_x)^2} - \frac{\omega_x(3\omega_0-\omega_x)\Omega_x^2}{2(\omega_0+\omega_x)^5} - \frac{\omega_x\left(40\omega_0^2 - 22\omega_0\omega_x + \omega_x^2\right)\Omega_x^4}{12(\omega_0+\omega_x)^8}. \tag{B8}$$

[1] S. Ashhab, J. R. Johansson, A. M. Zagoskin, and F. Nori, Phys. Rev. A **75**, 063414 (2007).
[2] S.-K. Son, S. Han, and S.-I. Chu, Phys. Rev. A **79**, 032301 (2009).
[3] S. N. Shevchenko, S. Ashhab, and F. Nori, Phys. Rep. **492**, 1 (2009).
[4] J. Hausinger and M. Grifoni, Phys. Rev. A **81**, 022117 (2010).
[5] E. Barnes and S. Das Sarma, Phys. Rev. Lett. **109**, 060401 (2012).
[6] J. Jing, L.-A. Wu, M. Byrd, J. Q. You, T. Yu, and Z.-M. Wang, Phys. Rev. Lett. **114**, 190502 (2015).
[7] J. Jing, P. H. Huang, and X. Hu, Phys. Rev. A **90**, 022118 (2014).
[8] F. Yoshihara, Y. Nakamura, F. Yan, S. Gustavsson, J. Bylander, W. D. Oliver, and J.-S. Tsai, Phys. Rev. B **89**, 020503 (2014).
[9] C. Deng, J.-L. Orgiazzi, F. Shen, S. Ashhab, and A. Lupascu, Phys. Rev. Lett. **115**, 133601 (2015).
[10] F. Yoshihara, T. Fuse, S. Ashhab, K. Kakuyanagi, S. Saito, and K. Semba, Phys. Rev. A **95**, 053824 (2017).
[11] F. Grossmann, T. Dittrich, P. Jung, and P. Hänggi, Phys. Rev. Lett. **67**, 516 (1991).
[12] F. Bloch and A. Siegert, Phys. Rev. **57**, 522 (1940).
[13] J. H. Shirley, Phys. Rev. **138**, B979 (1965).
[14] Z. G. Lü, Y. Y. Yan, H.-S. Goan, and H. Zheng, Phys. Rev. A **93**, 033803 (2016).
[15] Y. Song, J. P. Kestner, X. Wang, and S. Das Sarma, Phys. Rev. A **94**, 012321 (2016).
[16] Y.-C. Yang, S. N. Coppersmith, and M. Friesen, Phys. Rev. A **95**, 062321 (2017).
[17] M. O. Scully and M. S. Zubairy, *Quantum Optics* (Cambridge University Press, Cambridge, UK, 1997).
[18] P. K. Aravind and J. O. Hirschfelder, J. Phys. Chem. **88**, 4788 (1984).
[19] Z. G. Lü and H. Zheng, Phys. Rev. A **86**, 023831 (2012).
[20] Y. Y. Yan, Z. G. Lü, and H. Zheng, Phys. Rev. A **91**, 053834 (2015).
[21] P. Forn-Díaz, J. Lisenfeld, D. Marcos, J. J. García-Ripoll, E. Solano, C. J. P. M. Harmans, and J. E. Mooij, Phys. Rev. Lett. **105**, 237001 (2010).
[22] J. Tuorila, M. Silveri, M. Sillanpää, E. Thuneberg, Y. Makhlin, and P. Hakonen, Phys. Rev. Lett. **105**, 257003 (2010).
[23] R. Glenn, M. E. Limes, B. Pankovich, B. Saam, and M. E. Raikh, Phys. Rev. B **87**, 155128 (2013).
[24] J. Li, M. P. Silveri, K. S. Kumar, J. M. Pirkkalainen, A. Vepsäläinen, W. C. Chien, J. Tuorila, M. A. Sillanpää, P. J. Hakonen, E. V. Thuneberg *et al.*, Nat. Commun. **4**, 1420 (2013).
[25] S. Rohr, E. Dupont-Ferrier, B. Pigeau, P. Verlot, V. Jacques, and O. Arcizet, Phys. Rev. Lett. **112**, 010502 (2014).
[26] A. P. Saiko, G. G. Fedoruk, and S. A. Markevich, JETP Lett. **84**, 130 (2006).
[27] A. P. Saiko, R. Fedaruk, and S. A. Markevich, J. Phys. B **47**, 155502 (2014).
[28] Y. Y. Yan, Z. G. Lü, H. Zheng, and Y. Zhao, Phys. Rev. A **93**, 033812 (2016).
[29] C. Wei, A. S. M. Windsor, and N. B. Manson, J. Phys. B **30**, 4877 (1997).
[30] S. I. Chu and D. A. Telnov, Phys. Rep. **390**, 1 (2004).
[31] Y. Y. Yan, Z. G. Lü, and H. Zheng, Ann. Phys. **371**, 159 (2016).
[32] G. Teschl, *Ordinary Differential Equations and Dynamical Systems* (American Mathematical Society, Providence, RI, 2012).
[33] C. Cohen-Tannoudji, J. Dupont-Roc, and C. Fabre, J. Phys. B **6**, L218 (1973).
[34] C. Cohen-Tannoudji, J. Dupont-Roc, and G. Grynberg, *Atom-Photon Interactions: Basic Processes and Applications* (Wiley, New York, 2004).